IOP Publishing Journal of Physics: Condensed Matter
J. Phys.: Condens. Matter **32** (2020) 455702 (13pp) https://doi.org/10.1088/1361-648X/aba776

Multiband superconductors with degenerate excitation gaps

Paulo J F Cavalcanti[1], Tiago T Saraiva[2], J Albino Aguiar[1], A Vagov[3,4], M D Croitoru[1] and A A Shanenko[1,2,5]

[1] Departamento de Física, Universidade Federal de Pernambuco, Av. Prof. Aníbal Fernandes, s/n, 50740-560, Recife-PE, Brazil
[2] National Research University, Higher School of Economics, Moscow, 101000, Russia
[3] Institute for Theoretical Physics III, University of Bayreuth, Bayreuth 95440, Germany
[4] ITMO University, St. Petersburg, 197101, Russia

E-mail: arkadyshanenko@df.ufpe.br and shanenkoa@gmail.com

Received 15 May 2020, revised 7 July 2020
Accepted for publication 20 July 2020
Published 13 August 2020

Abstract

There is a tacit assumption that multiband superconductors are essentially the same as multigap superconductors. More precisely, it is usually assumed that the number of excitation gaps in the single-particle energy spectrum of a uniform superconductor (i.e. number of peaks in the density of states of the superconducting electrons) determines the number of contributing bands in the corresponding superconducting model. Here we demonstrate that contrary to this widely accepted viewpoint, the superconducting magnetic properties are sensitive to the number of contributing bands even when the spectral gaps are degenerate and cannot be distinguished. In particular, we find that the crossover between superconductivity types I and II—the intertype regime—is strongly affected by the difference between characteristic lengths of multiple contributing condensates. The reason for this is that condensates with diverse characteristic lengths, when coexisting in one system, interfere constructively or destructively, which results in multi-condensate magnetic phenomena regardless of the presence/absence of the multigap spectrum of a superconducting multiband material.

Keywords: multiband superconductors, superconducting properties, superconducting magnetic response

(Some figures may appear in colour only in the online journal)

1. Introduction

The concept of the multiband superconductivity was introduced in 1959 [1, 2] as a possible explanation of a multigap fine structure observed in frequency dependent conductivity of superconducting Pb and Hg, extracted from the infrared absorption spectrum [3]. Despite the long history of the concept and several other experimental results about the multigap character of some superconductors [4, 5], its detailed and unambiguous confirmation was obtained only in 2000s after experiments with MgB_2 (see, e.g., reference [6] and references therein). The observation of two well distinguished energy gaps in the excitation spectrum of MgB_2 [7, 8] [the density of states (DOS) of the superconducting electrons contains two peaks] ignited widespread interest in multiband superconductivity, boosting further experimental and theoretical studies. After a decade of intensive investigations, it became clear that multiple overlapping single-particle bands are present in many superconducting materials, ranging from iron-based [9] to organic high-T_c [10] and even topological superconductors [11, 12]. Recent first principle calculations have demonstrated that the Fermi surface of Pb comprises two Fermi sheets, confirming multiband nature of its superconducting state proposed [1] to explain pioneering experiments in [3].

It is widely assumed that a key marker for the multiband superconductivity is the appearance of multiple energy gaps in the single-particle spectrum of a homogeneous (bulk)

[5] Author to whom any correspondence should be addressed.

superconductor. Then, if the spectrum does not exhibit the multigap structure, the superconducting properties are expected to be those of single-band materials. More generally, it is usually assumed that the *number of spectral gaps determines the number of contributing bands* in a superconducting model that captures the essential physics of interest. A well-known example is MgB_2 which exhibits two spectral gaps associated with π and σ states [6–8]. Accordingly, theoretical models for superconductivity in MgB_2 consider two contributing bands (see, e.g., references [6, 13–19]) despite the fact that the first principle calculations reveal [20, 21] four single-particle bands for MgB_2, see also reference [6]. The two σ bands have different microscopic parameters (diverse Fermi sheets) but degenerate excitation gaps and the same holds for the π bands. A general perception is that the two-band model is sufficient to fully describe the superconducting state with the two spectral gaps.

However, there exists another approach that regards a multiband superconductor as a system governed by a set of *competing characteristic lengths* associated with different bands, see calculations of the healing lengths for different partial condensates in, e.g., references [18, 19, 22–25]. The single-particle spectrum of superconducting electrons is usually measured for bulk superconductors to avoid problems with the interpretation of nonuniform measurements. When the corresponding tunnelling measurements reveal, for example, a single peak in the DOS, it does not mean that the position-dependent gap functions of different contributing condensates are always the same. Their characteristic spatial lengths can be different due to peculiarities of the Fermi surface.

For clean systems (under consideration in the present work) such difference appears due to the presence of the band-dependent Fermi velocities. It is well-known that the Fermi velocity affects the condensate length in the single-band case. Similarly, the band-dependent Fermi velocities have an effect on the lengths of the partial condensates in multiband materials. However, here the physics is more complicated because of the interaction between the condensates. There is complex competition of the interband interactions with the disparity of the band Fermi velocities, and it becomes even more nontrivial in the presence of magnetic effects. In general, the disparity of the Fermi velocities increases the difference between the condensate lengths while the interband interactions support the so-called 'lengths-locking' regime (see the details of the 'lengths-locking' regime in [25]). Thus, the appearance of multiple characteristic lengths and the existence of many excitation gaps are both consequences of multiple sheets of the Fermi surface, interpreted as separate single-particle bands. However, these features appear on different levels of the theory—the system can have multiple energy gaps in the excitation spectrum but a single condensate length and, vice versa, a multiband superconductor can have multiple condensate lengths but a single spectral gap.

As is well known, the competition of different length-scales can lead to non-trivial physical consequences, e.g., to the spontaneous pattern formation [26]. Examples of systems with spontaneous patterns are well-known in the literature and include magnetic films [26, 27], liquid crystals [28], multilayer soft tissues [29], lipid monolayers [30], granular media [31] etc. A possibility of symmetry breaking patterns of vortices (labyrinth and stripes) induced by the presence of two condensate components with significantly different coherence lengths has recently attracted much interest in the context of unusual mixed (Shubnikov) phase configurations observed in MgB_2 (see, e.g., references [32, 33] and references therein). Coupled condensates coexisting in one material with diverse coherence lengths can interfere (interact) constructively or destructively, giving rise to phenomena absent in superconductors with a single-band condensate. In addition to the labyrinths and stripes of vortices mentioned above, other effects can be listed, e.g., chiral solitons [34–36], possible fractional vortices [37–42], hidden criticality [23], unusual oscillations in the current carrying state [43], enhancement of the intertype superconductivity [44, 45], unconventional Shapiro steps in the Josephson junctions [46, 47], the multiband vortex splitting effects [37, 48], a giant paramagnetic Meissner effect [49], multiband screening of superconducting fluctuations [50], gapless states and the related phase dependence of the excitation spectrum due to crossband pairing [51], etc.

In the present work we demonstrate that the crossover between superconductivity types I and II—the intertype (IT) regime (see, e.g., [44, 45])—is strongly affected by the difference between healing lengths of multiple contributing condensates even when the corresponding excitation gaps are degenerate and cannot be distinguished. Our analysis is done by using the formalism of the extended Ginzburg–Landau (EGL) theory [52, 53] generalized to the case of an arbitrary number of contributing bands. Here we consider systems in which the position-dependent gap functions associated with different contributing condensates have the same phases, i.e. there is no frustration related to the broken time-reversal symmetry, see e.g. [54–56]. The case of the gap functions with different phases [54–56] can also be appealing and can provide additional illustrations supporting our present conclusions. However, it requires a different variant of the EGL formalism and separate consideration.

The paper is organized as follows. In section 2 we discuss our formalism based on the τ-expansion of the microscopic equations, with $\tau = 1 - T/T_c$ the proximity to the critical temperature. It goes to one order beyond the standard Ginzburg–Landau (GL) approach, which is sufficient to describe a finite IT domain between types I and II in the phase diagram of the superconducting magnetic response. This formalism is then used in section 3, where boundaries of the IT domain are obtained for different configurations of the multiband structure. Conclusions are given in section 4.

2. Multiband EGL formalism

The EGL formalism is a convenient tool that can be employed when the physics beyond the GL theory is of interest but full microscopic calculations are impractical. A relevant example is the crossover between superconductivity types I and II—the IT regime. It is well known that within the GL theory, the crossover is reduced to a single point—it takes place at the

critical GL parameter [57–59] $\kappa = \kappa_0 = 1/\sqrt{2}$ ($\kappa = \lambda_{\rm L}/\xi_{\rm GL}$, where $\lambda_{\rm L}$ and $\xi_{\rm GL}$ are the London magnetic penetration depth and GL coherence length). However, as is known since 70s, this GL-based picture is valid only in the limit $T \to T_{\rm c}$ (more precisely, in the lowest order in τ). At $T < T_{\rm c}$ (beyond the lowest order in τ) there is a finite temperature-dependent crossover interval of κ's [60–76], which the GL theory does not capture. In the corresponding finite domain in the κ-T plain (the IT domain), the system has nonstandard field dependence of the magnetization [60–65] with unconventional spatial configurations of the mixed state [44, 61, 69–76], governed by long-range attraction of vortices [60–68] and many-vortex interactions [92]—the so-called intermediate mixed state.

For the derivation of the EGL formalism, we employ the M-band generalization of the two-band BCS model [1, 2] with the s-wave pairing in all contributing bands and the Josephson-like Cooper-pair transfer between the bands. For illustration, we consider a system in the clean limit and assume that all available bands have parabolic single-particle energy dispersions with 3D spherical Fermi surfaces. The pairing is controlled by the symmetric real coupling matrix $\check{g}$, with the elements $g_{\nu\nu'}$. The derivation of the formalism comprises two main steps: (1) the multiband Neumann–Tewordt (NT) functional is obtained from the microscopic model and (2) the τ-expansion is applied to reconstruct the NT functional. We outline main details of these steps, highlighting important differences in comparison with the two-band EGL approach [53]. The obtained formalism is then used in the analysis of the boundaries of the IT domain in the κ–T phase diagram.

2.1. Multiband Neumann–Tewordt functional

The NT functional [77, 78] is obtained from the microscopic expression for the condensate free energy by accounting for higher powers and higher gradients of the band-dependent gap functions $\Delta_\nu = \Delta_\nu(\mathbf{x})$, as compared to the GL functional. (Notice that from here on we use the notion 'gap function' for $\Delta_\nu(\mathbf{x})$ while the excitation or spectral gap is the feature of the single-particle spectrum of the uniform superconductor.) Only the terms giving the GL theory and its leading corrections are taken into account. The general expression for the free energy density of M-band s-wave superconductor (relative to that of the normal state at zero field) can be written as [44, 53]

$$f = \frac{\mathbf{B}^2}{8\pi} + \langle\vec{\Delta}, \check{g}^{-1}\vec{\Delta}\rangle + \sum_{\nu=1}^{M} f_\nu[\Delta_\nu], \tag{1}$$

where $\mathbf{B}$ is the magnetic field, $\vec{\Delta} = (\Delta_1, \Delta_2, \ldots, \Delta_M)$, $\langle\vec{a}, \vec{b}\rangle = \sum_\nu a_\nu^* b_\nu$ denotes the scalar product of vectors $\vec{a}$ and $\vec{b}$ in the band space, and the functional $f_\nu[\Delta_\nu]$ reads

$$f_\nu = -\sum_{n=0}^{\infty} \frac{1}{n+1} \int \prod_{j=1}^{2n+1} \mathrm{d}^3\mathbf{y}_j K_{\nu,2n+1}(\mathbf{x}, \{\mathbf{y}\}_{2n+1}) \times \Delta_\nu^*(\mathbf{x})\Delta_\nu(\mathbf{y}_1)\ldots\Delta_\nu^*(\mathbf{y}_{2n})\Delta_\nu(\mathbf{y}_{2n+1}), \tag{2}$$

with $\{\mathbf{y}\}_{2n+1} = \{\mathbf{y}_1, \ldots, \mathbf{y}_{2n+1}\}$. The integral kernels in equation (2) are given by (m is odd)

$$K_{\nu,m}(\mathbf{x}, \{\mathbf{y}\}_m) = -T\sum_\omega \mathcal{G}^{(B)}_{\nu,\omega}(\mathbf{x}, \mathbf{y}_1)\bar{\mathcal{G}}^{(B)}_{\nu,\omega}(\mathbf{y}_1, \mathbf{y}_2)\ldots \times \mathcal{G}^{(B)}_{\nu,\omega}(\mathbf{y}_{m-1}, \mathbf{y}_m)\bar{\mathcal{G}}^{(B)}_{\nu,\omega}(\mathbf{y}_m, \mathbf{x}), \tag{3}$$

where ω is the fermionic Matsubara frequency, $\mathcal{G}^{(B)}_{\nu,\omega}(\mathbf{x}, \mathbf{y})$ is the Fourier transform of the single-particle Green function calculated in the presence of the magnetic field and $\bar{\mathcal{G}}^{(B)}_{\nu,\omega}(\mathbf{x}, \mathbf{y}) = -\mathcal{G}^{(B)}_{\nu,-\omega}(\mathbf{y}, \mathbf{x})$. For $\mathcal{G}^{(B)}_{\nu,\omega}$ we employ the standard approximation sufficient to derive the extended GL theory

$$\mathcal{G}^{(B)}_{\nu,\omega}(\mathbf{x}, \mathbf{y}) = \exp\left[\mathrm{i}\frac{e}{\hbar\mathfrak{c}}\int_{\mathbf{y}}^{\mathbf{x}} \mathbf{A}(\mathbf{z})\cdot\mathrm{d}\mathbf{z}\right]\mathcal{G}^{(0)}_{\nu,\omega}(\mathbf{x}, \mathbf{y}), \tag{4}$$

where the integral in the exponent is taken along the classical trajectory of a charge carrier in a magnetic field with the vector potential $\mathbf{A}$. Here the Green function for zero field writes

$$\mathcal{G}^{(0)}_{\nu,\omega}(\mathbf{x}, \mathbf{y}) = \int \frac{\mathrm{d}^3\mathbf{k}}{(2\pi)^3}\frac{\exp[\mathrm{i}\mathbf{k}\cdot(\mathbf{x}-\mathbf{y})]}{\mathrm{i}\hbar\omega - \xi_\nu(\mathbf{k})}, \tag{5}$$

where the band-dependent single-particle energy dispersion reads

$$\xi_\nu(\mathbf{k}) = \xi_\nu(0) + \frac{\hbar^2\mathbf{k}^2}{2m_\nu} - \mu, \tag{6}$$

with m_ν the band effective mass, $\xi_\nu(0)$ the band lower edge, and μ the chemical potential.

To get simpler differential structure of the functional (1), one invokes the gradient expansion for the band gap functions and the vector potential as

$$\Delta_\nu(\mathbf{y}) = \Delta_\nu(\mathbf{x}) + ((\mathbf{y}-\mathbf{x})\cdot\boldsymbol{\nabla}_\mathbf{x})\Delta_\nu(\mathbf{x}) + \ldots,$$
$$\mathbf{A}(\mathbf{y}) = \mathbf{A}(\mathbf{x}) + ((\mathbf{y}-\mathbf{x})\cdot\boldsymbol{\nabla}_\mathbf{x})\mathbf{A}(\mathbf{x}) + \ldots, \tag{7}$$

which makes it possible to represent non-local integrals in f_ν as a series in powers of Δ_ν, its gradients and field spatial derivatives. The series are infinite and therefore a truncation procedure is needed. The GL theory follows from the standard Gor'kov truncation [79]. To incorporate the leading corrections to the GL formalism, one needs to go beyond the Gor'kov approximation. As the form of f_ν is not sensitive to the number of contributing bands, one can apply the truncation procedure to each of the band contributions separately and utilize the previous results derived for the single- and two-band cases, see reference [53]. The resulting multiband NT functional reads

$$f = \frac{\mathbf{B}^2}{8\pi} + \langle\vec{\Delta}, \check{g}^{-1}\vec{\Delta}\rangle + \sum_{\nu=1}^{M}\left\{\left[\mathcal{A}_\nu + a_\nu\left(\tau + \frac{\tau^2}{2}\right)\right]|\Delta_\nu|^2 + \frac{b_\nu}{2}(1+2\tau)|\Delta_\nu|^4 - \frac{c_\nu}{3}|\Delta_\nu|^6 + \mathcal{K}_\nu(1+2\tau)|\mathbf{D}\Delta_\nu|^2 - \mathcal{Q}_\nu\left(|\mathbf{D}^2\Delta_\nu|^2 + \frac{1}{3}\mathrm{rot}\,\mathbf{B}\cdot\mathbf{i}_\nu + \frac{4e^2}{\hbar^2\mathfrak{c}^2}\mathbf{B}^2|\Delta_\nu|^2\right) - \frac{\mathcal{L}_\nu}{2}\left[8|\Delta_\nu|^2|\mathbf{D}\Delta_\nu|^2 + \left(\Delta_\nu^{*2}(\mathbf{D}\Delta_\nu)^2 + \mathrm{c.c.}\right)\right]\right\}, \tag{8}$$

with $\mathbf{D} = \boldsymbol{\nabla} - \mathrm{i}(2e/\hbar\mathfrak{c})\mathbf{A}$ and $\mathbf{i}_\nu = (4e/\hbar\,\mathfrak{c})\,\mathrm{Im}\left[\Delta_\nu^* \mathbf{D}\Delta_\nu\right]$. The band dependent coefficients in equation (8) are

$$\mathcal{A}_\nu = N_\nu \ln\left(\frac{2e^\Gamma \hbar\omega_c}{\pi T_\mathrm{c}}\right), \quad a_\nu = -N_\nu, \quad b_\nu = N_\nu \frac{7\zeta(3)}{8\pi^2 T_\mathrm{c}^2},$$
$$c_\nu = N_\nu \frac{93\zeta(5)}{128\pi^4 T_\mathrm{c}^4}, \quad \mathcal{K}_\nu = \frac{b_\nu}{6}\hbar^2 v_\nu^2, \quad \mathcal{Q}_\nu = \frac{c_\nu}{30}\hbar^4 v_\nu^4,$$
$$\mathcal{L}_\nu = \frac{c_\nu}{9}\hbar^2 v_\nu^2, \tag{9}$$

where ω_c is the cut-off frequency, N_ν is the band DOS, v_ν denotes the band Fermi velocity, T_c is in the energy units, and $\zeta(\ldots)$ and Γ are the Riemann zeta-function and Euler constant.

The NT functional appears as a natural extension of the GL theory. The initial motivation of its derivation was to have an approach beyond the GL theory, which preserves, to some extent, the simplicity of the GL formalism. Such an approach is especially important in the case of spatially nonuniform problems. Unfortunately, the stationary point equations derived from the NT functional are rather complex even for the single-band case and not easier to solve than the original microscopic equations (see, e.g., equation (3) in reference [80]). Furthermore, these equations admit unphysical solutions [80] such as weakly damped oscillations of the condensate near the core of a single vortex state. The roots of this problem lie in the fact that the NT free energy functional is not bound from below because the coefficients c_ν, $\mathcal{Q}_\nu$, and $\mathcal{L}_\nu$ are positive. We also note in passing that a similar functional is commonly used in the analysis of the Fulde–Ferrel–Larkin–Ovchinnikov (FFLO) pairing (see, e.g., references [81–83]), however, in that case the sign of c_ν, $\mathcal{Q}_\nu$ and $\mathcal{L}_\nu$ is changed due the spin–magnetic interaction, which marks the appearance of the stable FFLO regime.

2.2. Perturbative τ-expansion

It was suggested for the single-band case (see reference [80] and references therein) that to eliminate the nonphysical solutions, the NT functional should be restructured by applying the perturbative τ-expansion, based on the fact that the fundamental small parameter of the microscopic equations is the proximity to the critical temperature τ. The stationary solution for the order parameter within the NT approach contains all odd powers of $\tau^{1/2}$ while the truncation of the infinite series in equation (3) does not distort only the two lowest orders $\tau^{1/2}$ (the GL term) and $\tau^{3/2}$ (the leading correction to the GL term). Incomplete higher-order terms in τ should be removed by means of the τ-expansion. A similar approach was subsequently applied to the two-band NT functional [53]. Here we generalize it to the case of an arbitrary number of contributing bands M.

Following this approach, we represent the band gap functions and fields in the form of τ-series [52, 53]

$$\Delta_\nu = \tau^{1/2}\left[\Delta_\nu^{(0)} + \tau\Delta_\nu^{(1)} + \ldots\right],$$
$$\mathbf{A} = \tau^{1/2}\left[\mathbf{A}^{(0)} + \tau\mathbf{A}^{(1)} + \ldots\right], \tag{10}$$
$$\mathbf{B} = \tau\left[\mathbf{B}^{(0)} + \tau\mathbf{B}^{(1)} + \ldots\right].$$

One also takes into account divergent condensate and field characteristic lengths $\propto\tau^{-1/2}$ that affect spatial gradients in the NT functional. This is formally done by introducing the spatial scaling as $\mathbf{x} \to \tau^{1/2}\mathbf{x}$ (see discussion after equation (10) in reference [52]). Notice that to get the stationary solution in the two lowest orders in τ, one also needs to operate with $\Delta_\nu^{(2)}$ but only in intermediate expressions.

Inserting equation (10) into equation (8) and applying the scaling $\mathbf{x} \to \tau^{1/2}\mathbf{x}$, one obtains the free energy density as

$$f = \tau^2\left[\tau^{-1}f^{(-1)} + f^{(0)} + \tau f^{(1)} + \ldots\right]. \tag{11}$$

Notice that the two lowest orders in the band gap functions and the field produce three lowest orders in the free energy but, as is shown below, the contribution $f^{(-1)}$ is zero for the stationary point. This contribution reads as

$$f^{(-1)} = \langle\vec{\Delta}^{(0)}, \check{L}\vec{\Delta}^{(0)}\rangle, \tag{12}$$

where the matrix elements of $\check{L}$ are defined as

$$L_{\nu\nu'} = g^{-1}_{\nu\nu'} - \mathcal{A}_\nu\delta_{\nu\nu'}, \tag{13}$$

with $g^{-1}_{\nu\nu'}$ being elements of the inverse coupling matrix $\check{g}^{-1}$ and $\delta_{\nu\nu'}$ denoting the Kronecker symbol. The next-order term $f^{(0)}$ is the GL functional

$$f^{(0)} = \frac{\mathbf{B}^{(0)2}}{8\pi} + \left(\langle\vec{\Delta}^{(0)}, \check{L}\vec{\Delta}^{(1)}\rangle + \mathrm{c.c.}\right) + \sum_{\nu=1}^{M} f_\nu^{(0)}, \tag{14}$$

where $f_\nu^{(0)}$ is given by

$$f_\nu^{(0)} = a_\nu|\Delta_\nu^{(0)}|^2 + \frac{b_\nu}{2}|\Delta_\nu^{(0)}|^4 + \mathcal{K}_\nu|\mathbf{D}^{(0)}\Delta_\nu^{(0)}|^2, \tag{15}$$

and $\mathbf{D}^{(0)} = \boldsymbol{\nabla} - \mathrm{i}(2e/\hbar\mathfrak{c})\mathbf{A}^{(0)}$. Finally, the highest-order term in equation (11) is given by

$$f^{(1)} = \frac{\mathbf{B}^{(0)}\cdot\mathbf{B}^{(1)}}{4\pi} + \left(\langle\vec{\Delta}^{(0)}, \check{L}\vec{\Delta}^{(2)}\rangle + \mathrm{c.c.}\right) + \langle\vec{\Delta}^{(1)}, \check{L}\vec{\Delta}^{(1)}\rangle + \sum_{\nu=1}^{M} f_\nu^{(1)}, \tag{16}$$

where

$$\begin{aligned} f_\nu^{(1)} = {} & \left(a_\nu + b_\nu|\Delta_\nu^{(0)}|^2\right)\left(\Delta_\nu^{(0)*}\Delta_\nu^{(1)} + \mathrm{c.c.}\right) + \frac{a_\nu}{2}|\Delta_\nu^{(0)}|^2 \\ & + b_\nu|\Delta_\nu^{(0)}|^4 - \frac{c_\nu}{3}|\Delta_\nu^{(0)}|^6 + 2\mathcal{K}_\nu|\mathbf{D}^{(0)}\Delta_\nu^{(0)}|^2 \\ & + \mathcal{K}_\nu\left[\left(\mathbf{D}^{(0)}\Delta_\nu^{(0)}\cdot\mathbf{D}^{(0)*}\Delta_\nu^{(1)*} + \mathrm{c.c.}\right) - \mathbf{A}^{(1)}\cdot\mathbf{i}_\nu^{(0)}\right] \\ & - \mathcal{Q}_\nu\left(|\mathbf{D}^{(0)2}\Delta_\nu^{(0)}|^2 + \frac{1}{3}\mathrm{rot}\,\mathbf{B}^{(0)}\cdot\mathbf{i}_\nu^{(0)} + \frac{4e^2\mathbf{B}^{(0)2}}{\hbar^2\mathfrak{c}^2}|\Delta_\nu^{(0)}|^2\right) \\ & - \frac{\mathcal{L}_\nu}{2}\left\{8|\Delta_\nu^{(0)}|^2|\mathbf{D}^{(0)}\Delta_\nu^{(0)}|^2 \right. \\ & \left. + \left[\Delta_\nu^{(0)2}(\mathbf{D}^{(0)*}\Delta_\nu^{(0)*})^2 + \mathrm{c.c.}\right]\right\}, \end{aligned} \tag{17}$$

and $\mathbf{i}_\nu^{(0)}$ is the lowest-order term in the τ-expansion of $\mathbf{i}_\nu$.

The τ-expansion of the NT functional is then used to derive a set of the stationary-point equations for the gap functions and

fields contributions—each of the equations correspond to a particular order of the τ-expansion. The equation in the lowest order reads

$$\frac{\delta\mathcal{F}^{(-1)}}{\delta\vec{\Delta}^{(0)\dagger}} = \check{L}\vec{\Delta}^{(0)} = 0, \tag{18}$$

where $\mathcal{F}^{(-1)}$ the free energy contribution obtained by integrating $f^{(-1)}$. This is the linearized gap equation in the multiband BCS theory that determines T_c. It has a nontrivial solution when

$$\det\ \check{L} = 0. \tag{19}$$

Recalling the definition of $\check{L}$, which includes $\mathcal{A}_\nu$ and, hence, depends on T_c, one sees that equation (19) determines zeros of an M-degree polynomial of the variable $\ln(2e^\Gamma\hbar\omega_c/\pi T_c)$. One should choose the smallest root of this polynomial, which gives the largest T_c. Here we assume that this solution is non-degenerate. This implies that the solution of the gap equation (18) corresponds to a one-dimensional irreducible representation of the system symmetry group. The opposite occurs in a particular case when the superconducting system has a symmetry additional to $U(1)$, which is reflected in a special symmetry of the matrix $\check{L}$ and results in the appearance of multi-component order parameter (see references [55, 84, 85]).

Once T_c is determined, it is convenient to introduce the eigenvalues and eigenvectors of $\check{L}$ as

$$\check{L}\vec{\epsilon} = 0 \tag{20}$$

with the zero eigenvalue and

$$\check{L}\vec{\eta}_i = \Lambda_i\vec{\eta}_i, \tag{21}$$

with nonzero eigenvalues $\Lambda_i \neq 0$. As the matrix $\check{L}$ is real and symmetric, the vectors $\vec{\epsilon}$ and $\vec{\eta}_i$ can be chosen such that they form an orthonormal basis so that $\langle\vec{\epsilon},\vec{\epsilon}\rangle = 1$, $\langle\vec{\epsilon},\vec{\eta}_i\rangle = 0$ and $\langle\vec{\eta}_i,\vec{\eta}_j\rangle = \delta_{ij}$. Then a general solution to the gap equation (18) reads in the form

$$\vec{\Delta}^{(0)} = \psi(\mathbf{x})\vec{\epsilon}, \tag{22}$$

where $\psi(\mathbf{x})$ controls the spatial profiles of all band condensates in the lowest order in τ.

The shape of $\psi(\mathbf{x})$ is governed by the stationary point equations associated with the GL functional (14). The first one of those is given by

$$\frac{\delta\mathcal{F}^{(0)}}{\delta\vec{\Delta}^{(0)\dagger}} = \check{L}\vec{\Delta}^{(1)} + \vec{W}[\vec{\Delta}^{(0)}] = 0, \tag{23}$$

where $\mathcal{F}^{(0)}$ is the free-energy term corresponding to $f^{(0)}$ and the components of $\vec{W}$ read

$$W_\nu = a_\nu\Delta_\nu^{(0)} + b_\nu\Delta^{(0)}|\Delta_\nu^{(0)}|^2 - \mathcal{K}_\nu\mathbf{D}^{(0)2}\Delta_\nu^{(0)}. \tag{24}$$

The second (Maxwell) equation is obtained as

$$\frac{\delta\mathcal{F}^{(0)}}{\delta\mathbf{A}^{(0)}} = \frac{1}{4\pi}\mathrm{rot}\,\mathbf{B}^{(0)} - \sum_{\nu=1}^{M}\mathcal{K}_\nu\mathbf{i}_\nu^{(0)} = 0. \tag{25}$$

Notice that the equation $\delta\mathcal{F}^{(0)}/\delta\vec{\Delta}^{(1)\dagger} = 0$ coincides with equation (18) while $\delta\mathcal{F}^{(0)}/\delta\mathbf{A}^{(1)} = 0$ is an identity relation because $\mathbf{A}^{(1)}$ does not contribute to $f^{(0)}$. By projecting equation (23) onto $\vec{\epsilon}$ and keeping in mind that $\vec{\epsilon}^{\dagger}\check{L} = 0$, one gets

$$a\psi + b\psi|\psi|^2 - \mathcal{K}\mathbf{D}^{(0)2}\psi = 0, \tag{26}$$

where coefficients a, b and $\mathcal{K}$ are averages over the contributing bands

$$a = \sum_{\nu=1}^{M} a_\nu|\epsilon_\nu|^2, \qquad b = \sum_{\nu=1}^{M} b_\nu|\epsilon_\nu|^4, \qquad \mathcal{K} = \sum_{\nu=1}^{M}\mathcal{K}_\nu|\epsilon_\nu|^2, \tag{27}$$

and ϵ_ν are the components of $\vec{\epsilon}$. Similarly, equation (25) is reduced to

$$\mathrm{rot}\ \mathbf{B}^{(0)} = 4\pi\mathcal{K}\mathbf{i}_\psi^{(0)}, \tag{28}$$

where $\mathbf{i}_\psi^{(0)}$ is obtained from $\mathbf{i}_\nu^{(0)}$ by substituting ψ for $\Delta_\nu^{(0)}$.

Therefore, the GL equations for the M-band system are given by equations (26) and (28). The corresponding condensate state is described by a single-component order parameter $\psi(\mathbf{x})$, in full agreement with the Landau theory in the case of a non-degenerate solution for T_c, see also references [16, 86, 87]. We note that the number of the components of the order parameter is determined by the dimensionality of the relevant irreducible representation of the corresponding symmetry group [57, 84], not by the number of the bands. The single-component order parameter means that the standard classification of the superconducting magnetic response is applied here: we have types I and II with the IT regime in between. The presence of multiple bands is reflected only in the expressions for the coefficients a, b and $\mathcal{K}$.

Using the eigenvectors of $\check{L}$ as the basis, we represent the next-to-leading contribution to the gap function as

$$\vec{\Delta}^{(1)} = \varphi(\mathbf{x})\vec{\epsilon} + \sum_{i=1}^{M-1}\varphi_i(\mathbf{x})\vec{\eta}_i, \tag{29}$$

with new position-dependent functions φ and φ_i to be found. Inserting equation (29) in equation (23), one obtains the equation

$$\sum_{i=1}^{M-1}\Lambda_i\varphi_i\vec{\eta}_i + \vec{W}[\vec{\Delta}^{(0)}] = 0. \tag{30}$$

Equation (30) is solved by projecting it onto $\vec{\eta}_j$, which yields $M-1$ equations for φ_j, i.e.,

$$\varphi_j = -\frac{1}{\Lambda_j}\left(\alpha_j\psi + \beta_j\psi|\psi|^2 - \Gamma_j\mathbf{D}^{(0)2}\psi\right), \tag{31}$$

where the coefficients α_j, β_j, and Γ_j are of the form

$$\alpha_j = \sum_{\nu=1}^{M} a_\nu\eta_{j\nu}^*\epsilon_\nu, \qquad \beta_j = \sum_{\nu=1}^{M} b_\nu\eta_{j\nu}^*\epsilon_\nu|\epsilon_\nu|^2,$$
$$\Gamma_j = \sum_{\nu=1}^{M}\mathcal{K}_\nu\eta_{j\nu}^*\epsilon_\nu, \tag{32}$$

and $\eta_{j\nu}$ are components of $\vec{\eta}_j$. Equations (29), (31), and (32) generalize the corresponding expressions for the two-band case [53]. One should keep in mind that the present formalism involves the eigenvectors of $\check{L}$ while $\vec{\Delta}^{(1)}$ in reference [53] was

represented as a linear combination of other explicitly chosen vectors. Therefore, to recover the expression for $\vec{\Delta}^{(1)}$ in reference [53], one needs to express $\vec{\epsilon}$ and $\vec{\eta}_j$ for $M = 2$ in terms of the vectors used in reference [53].

Thus, $M-1$ functions φ_i, which determine the second term for $\vec{\Delta}^{(1)}$ in equation (29), are found from the simple algebraic expressions (31) when using solutions to the GL equations (26) and (28). To find the first term in equation (29), that depends on φ and the leading correction to the field $\mathbf{A}^{(1)}$, one needs to solve the system of equations resulting from the projection of equation (30) onto the eigenvector $\vec{\epsilon}$ and zero functional derivatives of the free-energy contribution corresponding to $f^{(1)}$. However, as will be shown below, φ and $\mathbf{A}^{(1)}$ do not contribute to the boundaries of the IT domain. We note, however, that φ is necessary to calculate the band healing lengths—this calculation is outlined in the appendix A.

2.3. Free energy at the stationary point and thermodynamic critical field

The stationary free energy density is found by substituting the obtained stationary solutions into the corresponding expressions for the free energy functional, i.e.,

$$f_{\rm st} = \tau^2 \left[f_{\rm st}^{(0)} + \tau f_{\rm st}^{(1)} + \dots \right], \tag{33}$$

where the term of the order τ is absent by the virtue of equation (18) and the first non-vanishing contribution is the GL free energy

$$f_{\rm st}^{(0)} = \frac{\mathbf{B}^{(0)2}}{8\pi} + a|\psi|^2 + \frac{b}{2}|\psi|^4 + \mathcal{K}|\mathbf{D}^{(0)}\psi|^2, \tag{34}$$

we have also taken into account that $\langle \vec{\Delta}^{(0)}, \check{L}\vec{\Delta}^{(1)} \rangle = 0$, which follows from equation (18).

To find the leading order correction to the stationary GL free energy, we first rearrange the terms in $f^{(1)}$ that include $\Delta_\nu^{(1)}$ and $\Delta_\nu^{(1)*}$. For the stationary solution the sum of these terms in equation (16) can be represented as

$$\langle \vec{\Delta}^{(1)}, \check{L}\vec{\Delta}^{(1)} \rangle + \left(\langle \vec{\Delta}^{(1)}, \vec{W} \rangle + \text{c.c.} \right) = -\langle \vec{\Delta}^{(1)}, \check{L}\vec{\Delta}^{(1)} \rangle, \tag{35}$$

where equation (23) is taken into consideration. Using equations (26) and (31), we further obtain that $\langle \vec{\Delta}^{(1)}, \check{L}\vec{\Delta}^{(1)} \rangle$ can be expressed only in terms of ψ as

$$\langle \vec{\Delta}^{(1)}, \check{L}\vec{\Delta}^{(1)} \rangle = |\psi|^2 \sum_{i=1}^{M-1} \frac{a^2|\bar{\alpha}_i|^2}{\Lambda_i} + 2|\psi|^4 \sum_{i=1}^{M-1} \frac{ab\ \mathrm{Re}[\bar{\alpha}_i^* \bar{\beta}_i]}{\Lambda_i} + |\psi|^6 \sum_{i=1}^{M-1} \frac{b^2|\bar{\beta}_i|^2}{\Lambda_i}, \tag{36}$$

where the dimensionless parameters $\bar{\alpha}_i$ and $\bar{\beta}_i$ are defined by

$$\bar{\alpha}_i = \frac{\alpha_i}{a} - \frac{\Gamma_i}{\mathcal{K}}, \qquad \bar{\beta}_i = \frac{\beta_i}{b} - \frac{\Gamma_i}{\mathcal{K}}. \tag{37}$$

Then, $f^{(1)}$, given by equations (16) and (17), can be represented for the stationary solution in the form

$$\begin{aligned} f_{\rm st}^{(1)} = {} & \frac{\mathbf{B}^{(0)} \cdot \mathbf{B}^{(1)} - \mathbf{A}^{(1)} \cdot \mathrm{rot}\, \mathbf{B}^{(0)}}{4\pi} + \frac{\gamma_a}{2}|\psi|^2 \\ & + \gamma_b|\psi|^4 - \frac{\gamma_c}{3}|\psi|^6 + 2\mathcal{K}|\mathbf{D}^{(0)}\psi|^2 \\ & - \mathcal{Q}\left(|\mathbf{D}^{(0)2}\psi|^2 + \frac{1}{3}\mathrm{rot}\, \mathbf{B}^{(0)} \cdot \mathbf{i}_\psi^{(0)} + \frac{4e^2\mathbf{B}^{(0)2}}{\hbar^2 \mathfrak{c}^2}|\psi|^2 \right) \\ & - \frac{\mathcal{L}}{2}\left\{ 8|\psi|^2|\mathbf{D}^{(0)}\psi|^2 + \mathrm{Re}\left[\psi^2 \left(\mathbf{D}^{(0)*}\psi^* \right)^2 \right] \right\}, \end{aligned} \tag{38}$$

where

$$\mathcal{Q} = \sum_{\nu=1}^{M} \mathcal{Q}_\nu |\epsilon_\nu|^2, \qquad \mathcal{L} = \sum_{\nu=1}^{M} \mathcal{L}_\nu |\epsilon_\nu|^4, \qquad c = \sum_{\nu=1}^{M} c_\nu |\epsilon_\nu|^6. \tag{39}$$

and

$$\gamma_a = a - 2\sum_{i=1}^{M-1} \frac{a^2|\bar{\alpha}_i|^2}{\Lambda_i}, \qquad \gamma_b = b - 2\sum_{i=1}^{M-1} \frac{ab\ \mathrm{Re}[\bar{\alpha}_i^* \bar{\beta}_i]}{\Lambda_i}, \qquad \gamma_c = c + 3\sum_{i=1}^{M-1} \frac{b^2|\bar{\beta}_i|^2}{\Lambda_i}. \tag{40}$$

Using the above result, one can calculate the thermodynamic critical field $H_{\rm c}$ which is also sought in the form of the τ-expansion

$$H_{\rm c} = \tau \left[H_{\rm c}^{(0)} + \tau H_{\rm c}^{(1)} + \dots \right]. \tag{41}$$

By virtue of the definition, $H_{\rm c}$ can be obtained from

$$\frac{H_{\rm c}^2}{8\pi} = -f_{\rm st,0}, \tag{42}$$

where $f_{\rm st,0}$ is the free energy density of the Meissner state. In the lowest (GL) order, the uniform solution of equation (26) is given by $\psi_0 = \sqrt{|a|/b}$. This yields the corresponding contribution to the thermodynamic critical field as

$$H_{\rm c}^{(0)} = \sqrt{\frac{4\pi a^2}{b}}, \tag{43}$$

see equations (33), (34), and (41). $H_{\rm c}^{(0)}$ is formally the same as that for the single- and two-band cases [52, 53] but with the difference that a and b are now averages over M contributing bands. The next-order contribution to $H_{\rm c}$ is obtained from equations (33), (38), and (41), which gives

$$\frac{H_{\rm c}^{(1)}}{H_{\rm c}^{(0)}} = -\frac{1}{2} - \frac{ca}{3b^2} - \sum_{i=1}^{M-1} \frac{a}{\Lambda_i}|\bar{\alpha}_i - \bar{\beta}_i|^2. \tag{44}$$

Here the third term in the left-hand side has a different form as compared to the corresponding expressions for the single- and two-band cases in references [52, 53]. The origin of the differences has been already discussed after equation (32).

2.4. Gibbs free energy difference

A type I superconductor can only have a spatially uniform Meissner condensate state, which undergoes an abrupt transition to the normal state when the amplitude of the applied field **H** exceeds H_c. Type II superconductors, in addition to the Meissner phase, develop a nonuniform (mixed) state between the lower H_{c1} and upper H_{c2} critical fields, where $H_{c1} \leqslant H_c \leqslant H_{c2}$. A formal criterion for switching from type I to type II is that at $H = H_c$ the Meissner state becomes less energetically favourable than the mixed state. It is investigated by using the Gibbs free energy so that the switching criterion is obtained as the vanishing difference between the Gibbs free energies of the Meissner and nonuniform states. The Gibbs free energy density for a superconductor at $H = H_c$ is given by $g = f_{st} - H_c B/4\pi$, where **B** is directed along the external field **H** and found from the stationary-point equations for the corresponding condensate state. For the Meissner state we have $B = 0$ and $g = g_0 = f_{st,0} = -H_c^2/8\pi$. Thus, the density of the Gibbs free energy difference $\mathfrak{g} = g - g_0$ is written as

$$\mathfrak{g} = f_{st} - \frac{H_c B}{4\pi} + \frac{H_c^2}{8\pi}. \tag{45}$$

To calculate $\mathfrak{g}$, it is convenient to the use dimensionless quantities

$$\begin{aligned} &\tilde{\mathbf{x}} = \frac{\mathbf{x}}{\sqrt{2}\lambda}, \qquad \tilde{\mathbf{A}} = \kappa\frac{\mathbf{A}}{\lambda_L H_c^{(0)}}, \qquad \tilde{\mathbf{B}} = \sqrt{2}\kappa\frac{\mathbf{B}}{H_c^{(0)}}, \\ &\tilde{\psi} = \frac{\psi}{\psi_0}, \qquad \tilde{\mathfrak{g}} = \frac{4\pi\mathfrak{g}}{H^{(0)2}}, \qquad \tilde{G} = \frac{4\pi G}{H^{(0)2}(\sqrt{2}\lambda_L)^3}, \end{aligned} \tag{46}$$

where G is the integral of $\mathfrak{g}$ and

$$\lambda_L = \frac{\hbar\mathfrak{c}}{|e|}\sqrt{\frac{b}{32\pi K|a|}}, \qquad \kappa = \frac{\lambda_L}{\xi_{GL}} = \lambda_L\sqrt{\frac{|a|}{K}}. \tag{47}$$

We note that equation (47) differs from the conventional definitions for the GL coherence length ξ_{GL} and London penetration depth λ_L by the absence of the factor $\tau^{-1/2}$. This difference appears due to the scaling $\mathbf{x} \to \tau^{1/2}\mathbf{x}$ used in the derivation of the τ-expansion. Using the dimensionless units, we write the GL equations as

$$\psi - \psi|\psi|^2 + \frac{1}{2\kappa^2}\mathbf{D}^{(0)2}\psi = 0, \qquad \mathrm{rot}\,\mathbf{B}^{(0)} = \mathbf{i}_\psi^{(0)}, \tag{48}$$

$\mathbf{D}^{(0)} = \nabla + \mathrm{i}\mathbf{A}^{(0)}$, $\mathbf{i}_\psi^{(0)} = 2\ \mathrm{Im}\left[\psi\mathbf{D}^{(0)*}\psi^*\right]$ and the spatial gradients are also dimensionless. Hereafter we omit the tilde for brevity.

The τ-expansion for $\mathfrak{g}$ is obtained from equations (33), (34), (38), and (45) in the form

$$\mathfrak{g} = \tau^2\left[\mathfrak{g}^{(0)} + \tau\mathfrak{g}^{(1)} + \ldots\right], \tag{49}$$

where

$$\mathfrak{g}^{(0)} = \frac{1}{2}\left(1 - \frac{B^{(0)}}{\sqrt{2}\kappa}\right)^2 - |\psi|^2 + \frac{1}{2}|\psi|^4 + \frac{|\mathbf{D}^{(0)}\psi|^2}{2\kappa^2} \tag{50}$$

and

$$\begin{aligned} \mathfrak{g}^{(1)} = &\left(1 - \frac{B^{(0)}}{\sqrt{2}\kappa}\right)\left(\frac{\bar\gamma_a}{2} - \bar c\bar\gamma_c - \bar\gamma_b\right) - \frac{\bar\gamma_a}{2}|\psi|^2 + \bar\gamma_b|\psi|^4 \\ &+ \bar c\bar\gamma_c|\psi|^6 + \frac{|\mathbf{D}^{(0)}\psi|^2}{\kappa^2} + \frac{\bar{\mathcal{Q}}}{4\kappa^4}\left(|\mathbf{D}^{(0)2}\psi|^2 + \frac{\mathbf{i}_\psi^{(0)2}}{3} + \mathbf{B}^{(0)2}|\psi|^2\right) \\ &+ \frac{\bar{\mathcal{L}}}{4\kappa^2}\left\{8|\psi|^2|\mathbf{D}^{(0)}\psi|^2 + \mathrm{Re}\left[\psi^2\left(\mathbf{D}^{(0)*}\psi^*\right)^2\right]\right\}, \end{aligned} \tag{51}$$

where the dimensionless parameters are given by

$$\begin{aligned} &\bar c = \frac{ca}{3b^2}, \qquad \bar{\mathcal{Q}} = \frac{\mathcal{Q}a}{\mathcal{K}^2}, \qquad \bar{\mathcal{L}} = \frac{\mathcal{L}a}{\mathcal{K}b}, \qquad \bar\Lambda_j = \frac{\Lambda_j}{a}, \\ &\bar\gamma_a = \frac{\gamma_a}{a}, \qquad \bar\gamma_b = \frac{\gamma_b}{b}, \qquad \bar\gamma_c = \frac{\gamma_c}{c}. \end{aligned} \tag{52}$$

We note that to derive equation (51), we rearrange equation (38) by using the identity $\mathbf{A}^{(1)} \cdot \mathrm{rot}\ \mathbf{B}^{(0)} = \mathbf{A}^{(1)} \cdot \mathrm{rot}\ (\mathbf{B}^{(0)} - \mathbf{H}_c^{(0)})$. It is then integrated by parts, giving $\mathbf{B}^{(1)} \cdot (\mathbf{B}^{(0)} - \mathbf{H}_c^{(0)})$ while surface integrals vanish. This makes sure that the next-to-lowest order contribution to **B** does not appear in the Gibbs free energy difference, similarly to φ contributing to $\vec\Delta^{(1)}$. Thus, the Gibbs free energy difference, taken in the lowest and next-to-lowest orders in τ depends only on the solution to the GL equations. One also notes that the GL contribution $\mathfrak{g}^{(0)}$ is not sensitive to M which enters only its leading correction $\mathfrak{g}^{(1)}$.

2.5. B point and intertype domain

Integrating equation (49) yields the Gibbs free energy difference G. However, since the goal of our study is superconducting properties in the vicinity of the B point, in addition to the τ-expansion we apply the expansion with respect to $\delta\kappa = \kappa - \kappa_0$, which gives

$$\frac{G}{\tau^{1/2}} = G^{(0)} + \frac{\mathrm{d}G^{(0)}}{\mathrm{d}\kappa}\delta\kappa + G^{(1)}\tau, \tag{53}$$

where only the linear contributions in $\propto \delta\kappa$ and $\propto \tau$ are kept and the expansion coefficients are calculated at $\kappa = \kappa_0$. A significant advantage of this approach is that at κ_0 the GL theory simplifies considerably because the condensate-field configurations become self-dual being related by [88]

$$B^{(0)} = 1 - |\Psi|^2, \tag{54}$$

while the order parameter ψ satisfies the first order differential equation

$$\left(D_x^{(0)} - \mathrm{i}D_y^{(0)}\right)\psi = 0. \tag{55}$$

Here the field is taken along the z-direction so that ψ is not dependent on z and one can use $\mathbf{D}^{(0)2} = D_x^{(0)2} + D_y^{(0)2}$. Equations (54) and (55) are often referred to as the Bogomolnyi equations [88] (in the context of superconductivity they are also known as the Sarma solution [58]). Using these equations, one can demonstrate that the first contribution to the Gibbs free energy difference $G^{(0)}$ vanishes identically for any solution of the GL equations, which is a manifestation of the fact that at $H = H_c$ the self-dual GL theory is infinitely degenerate. The GL theory predicts that at κ_0 the normal state $\psi = 0$

is stable above H_c while below H_c the Meissner state $\psi = 1$ appears. Then, the mixed state appears only at $H = H_c$, hosting a plethora of exotic condensate-field configurations. Corrections to the GL theory break the degeneracy and successive self-dual configurations of the magnetic flux and condensate determine the properties of the IT mixed state.

With the Bogomolnyi equations, the Gibbs free energy difference given by equation (53) is reduced to

$$\frac{G}{\tau^{1/2}L} = -\sqrt{2}\,\mathcal{I}\,\delta\kappa + (\mathcal{I}\mathcal{A} + \mathcal{J}\mathcal{B})\,\tau, \tag{56}$$

where L is the system size along the direction of the field, $\mathcal{I}$ and $\mathcal{J}$ are given by the integrals

$$\mathcal{I} = \int \mathrm{d}^3\mathbf{x}|\psi|^2\left(1-|\psi|^2\right), \qquad \mathcal{J} = \int \mathrm{d}^3\mathbf{x}|\psi|^4\left(1-|\psi|^2\right), \tag{57}$$

while coefficients $\mathcal{A}$ and $\mathcal{B}$ are given by

$$\mathcal{A} = 2(1+\bar{\mathcal{Q}}) - \bar{\gamma}_b - \bar{c}\bar{\gamma}_c, \qquad \mathcal{B} = 2\bar{\mathcal{L}} - \frac{5}{3}\bar{\mathcal{Q}} - \bar{c}\bar{\gamma}_c. \tag{58}$$

Apart from the constants, that depend on M contributing bands, this expression for the Gibbs free energy difference is the same as obtained earlier for single- and two-band superconductors [44].

Now we have everything at our disposal to determine the boundaries of the IT domain on the κ–T plane. Its lower boundary $\kappa^*_{\mathrm{min}}(T)$ separates type I and IT regimes and marks the appearance/disappearance of the mixed state [44]. At this boundary the upper critical field H_{c2} approaches H_c. The condensate vanishes at H_{c2} and so the Gibbs free energies of the normal and condensate states become equal. At the same time the normal and Meissner states have the same Gibbs free energy at H_c. Therefore, the lower boundary of the IT domain is found from the criterion $G = 0$ taken together with the condition $\psi \to 0$. The latter means $\mathcal{J}/\mathcal{I} = 0$ in equation (56). Then one finds

$$\kappa^*_{\mathrm{min}} = \kappa_0(1 + \tau\mathcal{A}). \tag{59}$$

The upper boundary $\kappa^*_{\mathrm{max}}(T)$ separates type II and IT regimes and is determined by changing the sign of the long range interaction between vortices [44]—it is repulsive in type II and attractive in the IT domain. In order to calculate $\kappa^*_{\mathrm{max}}(T)$, one finds the asymptote of the GL solution for two vortices at large distance between them. The position dependent part of this asymptotic solution is plugged into equation (56), which yields the long-range interaction potential between two vortices. As the scaled GL equations (48) are independent of the number of contributing bands, one can adopt the long-range asymptote of the two-vortex solution ψ found previously in the two-band case [44], which yields $\mathcal{J}/\mathcal{I} = 2$. Then, the upper boundary is obtained as

$$\kappa^*_{\mathrm{max}} = \kappa_0\left[1 + \tau\left(\mathcal{A} + 2\mathcal{B}\right)\right]. \tag{60}$$

3. Role of multiple bands

3.1. General observations

A transparent structure of all contributions in the EGL formalism makes it possible to obtain important preliminary results before calculating κ^*_{min} and κ^*_{max}. The most significant observation is that the multigap structure and the disparity between characteristic lengths of different band condensates appear on different levels of the theory, leading to different physical consequences. Multiple excitation gaps appear in the lowest order in τ of the EGL theory: following equation (22), a multiband superconductor in the GL regime has, in general, multiple excitation gaps while the contributing band condensates are governed by the unique GL coherence length ξ_{GL}. Thus, on the level of the GL theory superconducting magnetic properties of a multiband system are the same as those of the single-band superconductor having the only energy gap in the excitation spectrum.

Differences between the condensate characteristic lengths and, thus, between spatial profiles of different band condensates appear only when the corrections to the GL theory are taken into account, i.e., in the next-to-lowest order in τ. Using the EGL approach, one calculates the band condensate healing lengths, to find a band-dependent leading correction to ξ_{GL} as $|\xi_\nu - \xi_{\nu'}| \propto \tau\xi_{\mathrm{GL}}$ (see appendix A and reference [24]). Thus, one can expect that phenomena associated with the disparity between the band condensate lengths are notable only at sufficiently low temperatures.

However, an important exception is the vicinity of the B point, i.e., the IT domain between types I and II. Here the GL theory is close to degeneracy and the next-to-lowest corrections in τ (and, thus, the difference between the band condensate lengths) play a crucial role in shaping the superconducting magnetic properties. In this case the mixed state becomes very sensitive to all characteristics of the multiband system, including the number of contributing bands and parameters of multiple Fermi sheets comprising the complex Fermi surface. The multiband structure can, therefore, have a notable effect on the IT domain, justifying the focus of this work.

It is also of significance, that the number of the energy gaps in the excitation spectrum of a uniform multiband superconductor is not always equal to the number of the contributing bands M, which can be seen from the corresponding gap equation

$$\Delta_\nu = \sum_{\nu'=1}^{M}\lambda_{\nu\nu'}n_{\nu'}\int_0^{\hbar\omega_c}\mathrm{d}\varepsilon\,\frac{\Delta_{\nu'}}{E_{\nu'}}\left[1-2f(E_{\nu'})\right], \tag{61}$$

where $E_\nu = \sqrt{\varepsilon^2 + |\Delta_\nu|^2}$ is the single-particle excitation energy, $\lambda_{\nu\nu'} = g_{\nu\nu'}N$ denotes the dimensionless coupling constant, $N = \sum_\nu N_\nu$ is the total single-particle DOS, $n_\nu = N_\nu/N$ is the relative DOS for band ν, $f(E_\nu)$ is the Fermi distribution function. For example, all the excitation gaps $\Delta_\nu = \Delta_\nu(T)$ (i.e., the gap functions for the uniform case) become

degenerate when the quantity

$$D_\nu = \sum_{\nu'=1}^{M} \lambda_{\nu\nu'} n_{\nu'} \tag{62}$$

assumes the same value for all contributing bands.

3.2. Microscopic parameters

The IT domain boundaries $\kappa^*_{\rm min}$ and $\kappa^*_{\rm max}$ depend on the following microscopic parameters: the dimensionless couplings $\lambda_{\nu\nu'} = g_{\nu\nu'}N$ (with $N = \sum_\nu N_\nu$ the total DOS), the relative band DOSs $n_\nu = N_\nu/N$, and the band velocities ratios v_ν/v_1. Since $T_{\rm c} \propto \hbar\omega_{\rm c}$, the cut-off frequency $\omega_{\rm c}$ does not contribute to $\kappa^*_{\rm min}$ and $\kappa^*_{\rm max}$.

For the calculations we choose realistic values of the parameters, recalling that in two-band superconductors the intraband dimensionless couplings are typically in the range 0.2–0.7 while the interband coupling is much smaller (see reference [44] and references therein). The relative band DOSs are usually similar for all bands so below we use $n_\nu = 1/M$ for any ν. The range of v_ν/v_1 can be estimated from the first principle calculations as well as from the ARPES measurements. For example, the angle-averaged Fermi velocities in the a–b plane of MgB_2 are calculated from first principles as $v_\sigma^{(a-b)} = 4.4 \times 10^5$ m s^{-1} for the σ states and $v_\pi^{(a-b)} = 5.35 \times 10^5$ m s^{-1} for the π states [89]. However, for the c-direction such calculations yield $v_\sigma^{(c)} = 7 \times 10^4$ m s^{-1} which is by an order of magnitude smaller than $v_\pi^{(c)} = 6 \times 10^5$ m s^{-1}. In addition, ARPES measurements for iron chalcogenide $FeSe_{0.35}Te_{0.65}$ have revealed three contributing bands with the maximal ratio of the band Fermi velocities close to 4 (see reference [90] and discussion in reference [24]).

In order to illustrate the role of the multiband structure in the presence of degenerate gaps, we consider models with one and two spectral gaps. In particular, in figure 1 for the one-band system we use $\lambda = 0.35$ whereas for the two-band system $\lambda_{11} = \lambda_{22} = 0.3$, $\lambda_{12} = 0.05$ ($n_\nu = 1/2$, as mentioned in the previous paragraph). This choice ensures that the both variants exhibit the same single energy gap in the excitation spectrum. In figure 2 we consider multiband superconductors comprising M contributing bands, with $M = 3, 4, 5$. The dimensionless couplings are chosen so that to get the same single excitation gap as in figure 1, namely, we adopt $\lambda_{\nu\neq\nu'} = 0.05$ and $\lambda_{\nu\nu} = 0.35 - 0.05(M-1)$. In this case D_ν given by equation (62) does not depend on ν (with $n_\nu = 1/M$). To consider the two-gap case, we investigate the two- and four-band materials, see figure 3. We take $\lambda_{11} = 0.175, \lambda_{22} = 0.125, \lambda_{12} = 0.05$ for the two-band system and $\lambda_{11} = \lambda_{22} = 0.3$, $\lambda_{33} = \lambda_{44} = 0.2$ and $\lambda_{\nu\neq\nu'} = 0.05$ for the four-band superconductor; the relative band DOSs for all contributing bands are assumed equal. To illustrate variations in the boundaries of the IT domain, we assume that the relative Fermi velocities depend on the variable parameter β. For the two band system in figures 1 and 3 we use $\beta = v_2/v_1$. For the M-band models in figure 2 we set $\beta = v_2/v_1$ and $v_\nu = v_2$ for $\nu > 2$. Finally, for the four-band model in figure 3 we utilize a more complicated parametrization $\beta = v_2/v_1 = v_3/v_1 = v_4/2v_1$. We stress that our qualitative conclusions do not depend on a particular choice of the microscopic parameters.

3.3. Numerical results for the IT domain boundaries

Using the chosen microscopic parameters, we examine excitation gaps, the boundaries of the IT domain as well as the condensate healing lengths for superconductors with one, two and four bands.

Figure 1 illustrates a comparison between the one- and two-band models. The both models exhibit the same single energy gap in the excitation spectrum, as shown in figure 1(a). However, the difference between them is apparent in figure 1(b) which shows $\mathrm{d}\kappa^*_{\rm min}/\mathrm{d}\tau$ and $\mathrm{d}\kappa^*_{\rm max}/\mathrm{d}\tau$ as functions of the Fermi velocities ratio $\beta = v_2/v_1$. The calculation reveals a notable dependence of the IT domain boundaries of the two-band model on β (dotted lines) in comparison with the one-band case, for which the IT boundaries are given by the material-independent constants −0.29 and 0.67, [44] as illustrated by solid lines. The difference between the two cases is maximal in the limits $\beta \ll 1$ and $\beta \gg 1$ but disappears when $\beta = 1$.

To clarify the physical roots of the obtained results, we utilize the formalism of reference [24] (for reader's convenience, outlined in appendix A), and calculate the derivative $\mathrm{d}|\xi_2 - \xi_1|/\mathrm{d}\tau$, where $|\xi_2 - \xi_1|$ is the absolute value of the difference of the band healing lengths ξ_2 and ξ_1 for the two-band system in question. To the next-to-lowest order in τ, we have $\xi_\nu = \xi_\nu^{(0)} + \tau\xi_\nu^{(1)}$, with $\xi_\nu^{(0)} = \xi_{\rm GL}$, see references [24, 53, 86, 87]. (This healing-length expression should be multiplied by $\tau^{-1/2}$ to return to the standard definition.) Therefore, taken to one order beyond the GL theory, $\mathrm{d}|\xi_2 - \xi_1|/\mathrm{d}\tau$ is equal to $|\xi_2^{(1)} - \xi_2^{(1)}|$ and is not τ-dependent. The result is given in figure 1(c) in units of the GL coherence length $\xi_{\rm GL}$. Comparing figures 1(b) and (c) demonstrates that the size of the IT domain closely follows the healing length difference—the domain size grows with increasing the difference. One can thus see that even though the two-band system has a single gap in its excitation spectrum, its magnetic properties are strongly affected by the presence of multiple condensates with different characteristic lengths and, in general, differ significantly from those of the single-band case. The only exception is the case of $\xi_1 = \xi_2$, when the excitation spectra and magnetic properties of the single- and two-band systems become indistinguishable. At this point the quantity $\mathrm{d}|\xi_2 - \xi_1|/\mathrm{d}\tau$ exhibits a pronounced minimum at which the slope of $\mathrm{d}|\xi_2 - \xi_1|/\mathrm{d}\tau$, as a function of β, changes its sign abruptly. Notice that this discontinuity of the derivative with respect to β is not a consequence of any phase transition but appears because the lengths ξ_1 and ξ_2 cross each other at $\beta = 1$.

To gain a further insight, figure 2 demonstrates the boundaries of the IT domain for multiband superconductors with the number of the contributing bands $M = 3, 4, 5$. These multiband superconductors have the only excitation gap being the same as in figure 1. One observes that the IT domain boundaries are sensitive to a particular value of M so that the results are different from those for the one-band and two-band models. This difference is pronounced for $\beta \ll 1$ and $\beta \gg 1$, i.e. when the characteristic lengths of the partial condensates deviate significantly from each other. Due to the choice of the band Fermi velocities, we have two distinguished condensate lengths ξ_1 and ξ_2, the latter is equal to ξ_ν with $\nu > 2$. Similarly

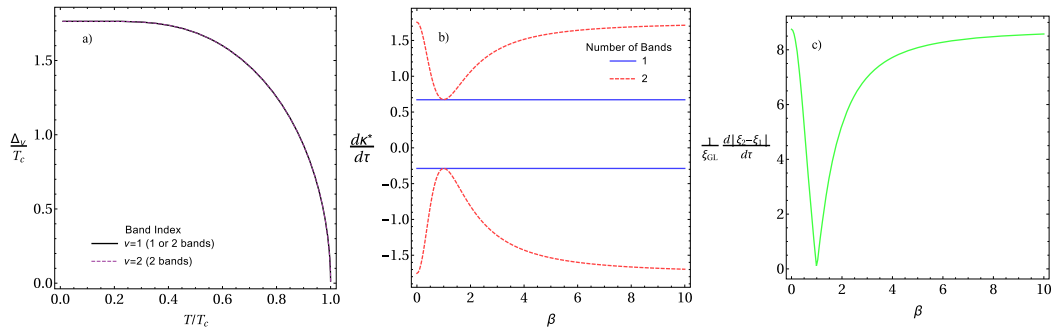

Figure 1. Results for one- and two-band superconductors with the microscopic parameters given in section 3.2, chosen so that both materials have the same excitation gap, degenerate for the two-band system, shown in panel (a) as a function of T (in units of T_c). Panel (b) plots slopes of the IT domain boundaries $d\kappa^*_{max}/d\tau$ (two upper lines) and $d\kappa^*_{min}/d\tau$ (two lower lines) versus $\beta = v_2/v_1$ for the two-band (dotted) and single-band (solid) cases, the single-band results are material independent quantities -0.29 and 0.67. Panel (c) shows the derivative $d|\xi_2 - \xi_1|/d\tau$ versus β, where $|\xi_2 - \xi_1|$ is the absolute value of the difference of the band healings lengths ξ_2 and ξ_1 for the two-band system in question.

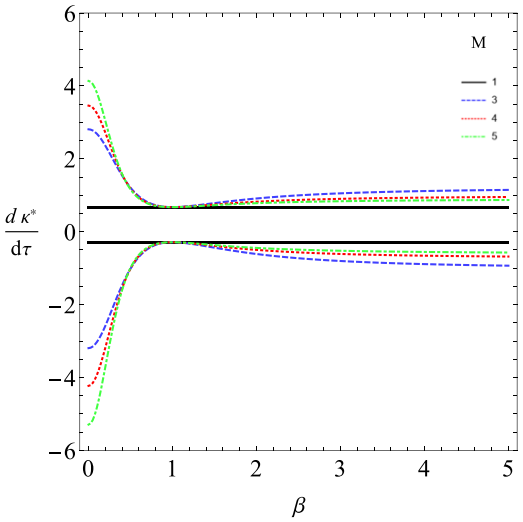

Figure 2. The slopes of the IT domain boundaries $d\kappa^*_{max}/d\tau$ (upper lines) and $d\kappa^*_{min}/d\tau$ (lower lines) for the case of a single spectral gap in the model with the number of bands $M = 3$ (dashed line), $M = 4$ (dotted) and $M = 5$ (dashed-dotted). The microscopic parameters are discussed in section 3.2 and chosen so that all the given materials have the same temperature-dependent gap as in figure 1. The results are versus $\beta = v_2/v_1$, with $v_\nu = v_2$ for $\nu > 2$; the single-band boundaries are the universal constants -0.29 and 0.67 shown as a guide for the eye by the solid line.

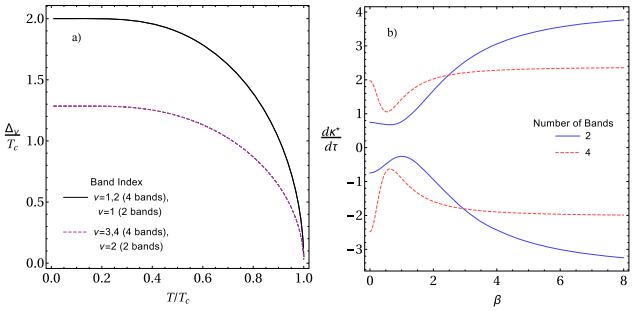

Figure 3. Results for two- and four-band materials, calculated with the microscopic parameters given in section 3.2 and chosen such that both materials have two excitation gaps. Panel (a) shows the gaps versus temperature (in units of T_c). Panel (b) plots slopes of the IT domain boundaries $d\kappa^*_{max}/d\tau$ (two upper lines) and $d\kappa^*_{min}/d\tau$ (two lower lines) as functions of $\beta = v_2/v_1$ (for the two-band case, solid lines) and $\beta = v_2/v_1 = v_3/v_1 = v_4/2v_1$ (for the four-band system, dashed lines).

to figure 1, when $\xi_1 = \xi_2$, i.e. for $\beta = 1$, the IT boundaries of the M-band model approach the boundaries of the IT domain for the one-band model. One sees again that the crossover between types I and II is determined by the number of contributing bands and by the interplay of the related condensate characteristic lengths. Obviously, the IT behavior cannot be captured by the model with the number of bands equal to the number of gaps in the single-particle spectrum of the uniform superconductor.

A further illustration is given in figure 3 which compares results for the two- and four-band systems. The parameters are chosen such that both systems have the same two excitation gaps (see figure 3(a)). In particular, spectral gaps are degenerate for bands 1, 2 and 2, 3 in the four-band case. The IT domain boundaries (their τ-derivatives) for the two-band system are shown in figure 3(b) versus $\beta = v_2/v_1$ by solid lines. One can see that in general, the corresponding IT domain is significantly different from the two-band IT domain shown in figure 1(b), which is a consequence of the two excitation gaps in the present case. However, the two-band IT boundaries in figure 3(b) are still close to the single-band ones in vicinity of $\beta = 1$. Here the difference between the healing lengths ξ_1 and ξ_2 is minimal and the two-band system exhibits a nearly single-band superconducting magnetic response, despite the presence of two excitation gaps. We again observe that the presence/absence of diverse characteristic lengths of multiple condensates coexisting in one material is more essential for the superconducting magnetic properties than the presence/absence of multiple gaps in the excitation spectrum of the uniform superconductor.

The quantities $d\kappa^*_{max}/d\tau$ and $d\kappa^*_{min}/d\tau$ for the four-band system are given by dotted lines in figure 3(b) versus $\beta = v_2/v_1 = v_2/v_1 = v_4/2v_1$. One sees that the IT domain boundaries for the four-band case are close to the two-band IT bound-

aries at $\beta \sim 3$. For $\beta \gtrsim 3$ the size of the IT domain for the two-band system is notably larger and, on the contrary, for $\beta \lesssim 3$ the IT domain is larger in the four-band case. One also notes that unlike the two-band case the IT domain for the four-band system in figure 3(b) never approaches the single-band result (cf figure 1(b)). In general, one can expect that the larger is the number of competing superconducting condensates with different characteristics, the more significant are the deviations from the single-condensate physics.

4. Conclusions

In this work we have demonstrated that the presence of multiple competing lengths, each connected with corresponding partial condensate, is a more fundamental feature of a multiband superconductor for its magnetic properties than the presence of multiple gaps in the excitation spectrum. This is illustrated by considering boundaries of the IT domain in the phase diagram of the superconducting magnetic response. For example, our results have revealed that a superconductor can have many gaps in the excitation spectrum while exhibiting standard magnetic properties of a single-band material. There is also a reverse situation, when a superconductor has a single energy gap in the excitation spectrum but multiple competing characteristic lengths of contributing band condensates, which results in notable changes of the superconducting magnetic properties in the IT regime as compared to the single-band case. Generally, our analysis shows that the multi-condensate physics can appear irrespective of the presence/absence of multiple spectral gaps. Two superconductors with different numbers of the contributing bands but with the same energy gaps in their excitation spectra (some of the spectral gaps are degenerate) can exhibit different magnetic properties sensitive to the spatial scales of the band condensates. This discrepancy between different manifestations of multiple bands in superconducting materials must be taken into account in analysis of experimental data and, generally, in studies of multiband superconductors. In addition, given the significant advances in chemical engineering of various materials, including multiband superconductors, it is of great importance to search for systems that enrich our knowledge of and understanding the physics of the materials. Multiband superconductors with degenerate excitation gaps can be a good example of such systems, clearly demonstrating that 'multiband' can be dramatically different from 'multigap'.

Our analysis has been performed within the EGL approach that takes into account the leading corrections to the GL theory in the perturbative expansion of the microscopic equations in $\tau = 1 - T/T_c$. This formalism, previously constructed for single- and two-band systems, has been extended in the present work to the case of an arbitrary number of contributing bands. Its advantage is that it allows one to clearly distinguish various effects appearing due to the multiband structure in different types of superconducting characteristics. It particular, it reveals solid correlations between changes in the IT domain with the competition of multiple characteristic lengths of the contributing condensates.

Acknowledgments

This work was supported by Brazilian agencies, Conselho Nacional de Ciência e Tecnologia (CNPq), Grant No. 309374/2016-2 and Fundação de Amparo a Ciência e Tecnologia do Estado de Pernambuco (FACEPE) Grant No. APQ-0936-1.05/15. PJFC thanks CAPES Programa de Doutorado Sanduíche no Exterior, Processo No. 88881.186964/2018-01. TTS and AV acknowledge hospitality of Departamento de Física da Universidade Federal de Pernambuco during their temporary stays in 2018 and support from CNPq Grant No. 400510/2014-6 and FACEPE. MDC acknowledges the Departamento de Física da Universidade Federal de Pernambuco for visiting professor fellowship in 2019, Grant Propesq 05.2018-031782/2018-88.

Appendix A. Leading correction to the GL coherence length

He we employ the EGL approach to calculate the band dependent healing lengths ξ_ν up to the leading corrections to the GL coherence length. The GL theory of multiband superconductors has a single order parameter which yields equal healing lengths for different band condensates. (A multiband superconductor can have more than one order parameter in the GL regime when the solution of the linearized gap equation for T_c is degenerate [55]; this case is not considered here.) However, when one takes into account the leading corrections to GL theory, band healing lengths become different. These corrections have been calculated earlier [24] for the one-band and two-band systems, and we now recall those results and extend them to the case of an arbitrary number of contributing bands.

We consider the condensate that occupies a half space $x > 0$ and is suppressed for $x \leqslant 0$. Each band condensate recovers its bulk value in a distance (measured from the interface $x = 0$) that is called the band healing length ξ_ν. This length is defined from the criterion

$$\frac{\Delta_\nu(\xi_\nu)}{\Delta_\nu(\infty)} = \frac{\Delta_\nu^{(0)}(\xi_\nu^{(0)})}{\Delta_\nu^{(0)}(\infty)}, \tag{A.1}$$

where ξ_ν is given by the τ-expansion

$$\xi_\nu = \xi_\nu^{(0)}\left(1 + \tau\xi_\nu^{(1)}\right), \tag{A.2}$$

and, taken in the lowest order in τ, the band healing length coincides with the GL coherence length $\xi_\nu^{(0)} = \xi_{GL}$. We solve the GL equation (48) without magnetic field and with the boundary conditions $\psi(0) = \psi'(\infty) = 0$, with ψ' the first derivative with respect to x measured in units of ξ_{GL}. The well-known solution reads as [91]

$$\psi = \tanh\left(x/\sqrt{2}\right), \tag{A.3}$$

where ψ is given in units of $\psi_0 = \sqrt{|a|/b}$. One sees from equation (22) that ψ controls $\vec{\Delta}^{(0)}$.

The next-to-lowest contribution to Δ_ν is given by equation (29). In this equation φ_j are explicitly expressed via

ψ by equation (31) but φ should be obtained from the stationary equation $\delta\mathcal{F}^{(1)}/\delta\vec{\Delta}^{(0)\dagger}=0$, where $\mathcal{F}^{(1)}$ corresponds to $f^{(1)}$ in equation (11). The projection of this equation onto the eigenvector $\vec{\epsilon}$ yields the equation for φ that can be written as

$$(1-3\psi^2)\varphi+\varphi''=A\psi+B\psi^3+C\psi^5+D\psi\psi'^2, \quad \text{(A.4)}$$

where φ is in units of ψ_0, φ'' is the second derivative with respect to the scaled variable x, and the coefficients read as

$$\begin{aligned}
A&=\frac{3}{2}+\bar{\mathcal{Q}}+\sum_{i=1}^{M-1}\frac{\bar{\alpha}_i^2}{\bar{\Lambda}_i},\\
B&=5\bar{\mathcal{L}}-4\bar{\mathcal{Q}}-2\sum_{i=1}^{M-1}\frac{\Gamma_i(\bar{\alpha}_i-\bar{\beta}_i)+2\mathcal{K}\bar{\alpha}_i\bar{\beta}_i}{\mathcal{K}\bar{\Lambda}_i},\\
C&=3\bar{c}+3\bar{\mathcal{Q}}-5\bar{\mathcal{L}}+3\sum_{i=1}^{M-1}\frac{\bar{\beta}_i^2}{\bar{\Lambda}_i},\\
D&=6\bar{\mathcal{Q}}-5\bar{\mathcal{L}}-6\sum_{i=1}^{M-1}\frac{\Gamma_i\bar{\beta}_i}{\mathcal{K}\bar{\Lambda}_i},
\end{aligned} \quad \text{(A.5)}$$

where $\mathcal{K}$, Γ_j, $\bar{c}$, $\bar{\mathcal{Q}}$, $\bar{\mathcal{L}}$, $\bar{\alpha}_j$, $\bar{\beta}_j$ and $\bar{\Lambda}_j$ are given by equations (27), (32), (37), and (52). Here we consider that vectors $\vec{\epsilon}$ and $\vec{\eta}_j$ have only real components, i.e., $\alpha_i=\alpha_i^*$, $\beta_i=\beta_i^*$, and $\Gamma_i=\Gamma_i^*$.

The solution of equation (A.4) at $\varphi(0)=\varphi'(\infty)=0$ is obtained as

$$\begin{aligned}
\varphi=&-\frac{3(A+B)+5C+D}{6}\tanh\left(\frac{x}{\sqrt{2}}\right)+\frac{2C+D}{6}\\
&\times\tanh^3\left(\frac{x}{\sqrt{2}}\right)-\frac{A-C}{2}\frac{x}{\sqrt{2}}\,\mathrm{sech}^2\left(\frac{x}{\sqrt{2}}\right).
\end{aligned} \quad \text{(A.6)}$$

Then, using equations (22), (29), (A.3), and (A.6), one finds

$$\xi_\nu^{(1)}=\frac{A-C}{2}+\sqrt{2}\psi\left(\frac{1}{\sqrt{2}}\right)\left(\frac{2C+D}{6}+\sum_{i=1}^{M-1}\frac{\bar{\beta}_i}{\bar{\Lambda}_i}\frac{\eta_{i\nu}}{\epsilon_\nu}\right). \quad \text{(A.7)}$$

We note that only the last term in this expression contributes to the difference between the healing lengths of two different bands ν and ν', so that

$$\xi_\nu-\xi_{\nu'}=0.86\,\tau\,\xi_{\mathrm{GL}}\sum_{i=1}^{M-1}\frac{\bar{\beta}_i}{\bar{\Lambda}_i}\left(\frac{\eta_{i\nu}}{\epsilon_\nu}-\frac{\eta_{i\nu'}}{\epsilon_{\nu'}}\right), \quad \text{(A.8)}$$

with $\psi(1/\sqrt{2})=0.86$.

Let us consider, for illustration, equation (A.7) for the two-band system with degenerate excitation gaps. In this case the eigenvector of the matrix $\check{L}$ with zero eigenvalue satisfies $\epsilon_1=\epsilon_2$. Then, for equal band Fermi velocities the parameter $\bar{\beta}_1=0$ as $\beta_1/b=\Gamma_1/\mathcal{K}$, see the definition of these quantities in section 2.2. Since only $i=1$ contributes to the sum in equation (A.7), we find $\xi_1^{(1)}=\xi_2^{(1)}$. Thus, the healing lengths ξ_1 and ξ_2 are the same (at least up to the leading correction to the GL theory), which is in agreement with the results given in figure 1(c), where the healing length difference drops to zero at $v_2=v_1$. The same conclusion can easily be obtained for $M>2$, when all excitation gaps are degenerate and the bands have the same Fermi velocity.

ORCID iDs

A A Shanenko https://orcid.org/0000-0002-6031-5106

References

[1] Suhl H, Matthias B T and Walker L R 1959 *Phys. Rev. Lett.* **3** 552–4
[2] Moskalenko V A 1959 *Phys. Met. Metallogr.* **8** 25–36
[3] Ginsberg D M, Richards P L and Tinkham M 1959 *Phys. Rev. Lett.* **3** 337–8
[4] Townsend P and Sutton J 1963 *Phys. Rev. Lett.* **11** 154–6
[5] Zavaritskii N V 1965 *Sov. Phys. - JETP* **21** 557–62
[6] Canfield P C and Crabtree G W 2003 *Phys. Today* **56** 34–40
[7] Szabó P, Samuely P, Kačmarčík J, Klein T, Marcus J, Fruchart D, Miraglia S, Marcenat C and Jansen A G M 2001 *Phys. Rev. Lett.* **87** 137005
[8] Iavarone M *et al* 2002 *Phys. Rev. Lett.* **89** 187002
[9] Paglione J and Greene R L 2010 *Nat. Phys.* **6** 645–58
[10] Mazziotti M V, Valletta A, Campi G, Innocenti D, Perali A and Bianconi A 2017 *Europhys. Lett.* **118** 37003
[11] Deng S, Viola L and Ortiz G 2012 *Phys. Rev. Lett.* **108** 036803
[12] Deng S, Ortiz G and Viola L 2013 *Phys. Rev.* B **87** 205414
[13] Askerzade İ N, Gencer A and Güçlü N 2002 *Supercond. Sci. Technol.* **15** L13–6
[14] Golubov A A, Kortus J, Dolgov O V, Jepsen O, Kong Y, Andersen O K, Gibson B J, Ahn K and Kremer R K 2002 *J. Phys.: Condens. Matter.* **14** 1353–60
[15] Gurevich A 2003 *Phys. Rev.* B **67** 184515
[16] Koshelev A E and Golubov A A 2004 *Phys. Rev. Lett.* **92** 107008
[17] Zhitomirsky M E and Dao V-H 2004 *Phys. Rev.* B **69** 054508
[18] Tanaka K, Agterberg D F, Kop J and Eschrig M 2006 *Phys. Rev.* B **73** 220501(R)
[19] Tanaka K, Eschrig M and Agterberg D F 2007 *Phys. Rev.* B **75** 214512
[20] Kortus J, Mazin I I, Belashchenko K D, Antropov V P and Boyer L L 2001 *Phys. Rev. Lett.* **86** 4656
[21] An J M and Pickett W E 2001 *Phys. Rev. Lett.* **86** 4366
[22] Komendová L, Milošević M V, Shanenko A A and Peeters F M 2011 *Phys. Rev.* B **84** 064522
[23] Komendová L, Chen Y, Shanenko A A, Milošević M V and Peeters F M 2012 *Phys. Rev. Lett.* **108** 207002
[24] Saraiva T T, de Souza Silva C C, Aguiar J A and Shanenko A A 2017 *Phys. Rev.* B **96** 134521
[25] Chen Y, Zhu H and Shanenko A A 2020 *Phys. Rev.* B **101** 215510
[26] Seul M and Wolfe R 1992 *Phys. Rev.* A **46** 7519–33
[27] Seul M and Andelman D 1995 *Science* **267** 476–83
[28] Maclennan J and Seul M 1992 *Phys. Rev. Lett.* **69** 2082–5
[29] Stoop N, Lagrange R, Terwagne D, Reis P M and Dunkel J 2015 *Nat. Mater.* **14** 337–42
[30] Keller S L and McConnell H M 1999 *Phys. Rev. Lett.* **82** 1602–5
[31] Aranson I S and Tsimring L S 2006 *Rev. Mod. Phys.* **78** 641–92
[32] Moshchalkov V, Menghini M, Nishio T, Chen Q H, Silhanek A V, Dao V H, Chibotaru L F, Zhigadlo N D and Karpinski J 2009 *Phys. Rev. Lett.* **102** 117001
[33] Curran P J, Desoky W M, Milošević M V, Chaves A, Laloë J-B, Moodera J S and Bending S J 2015 *Sci. Rep.* **5** 15569
[34] Tanaka Y 2001 *Phys. Rev. Lett.* **88** 017002
[35] Tanaka Y 2001 *J. Phys. Soc. Japan* **70** 2844–7
[36] Kuplevakhsky S V, Omelyanchouk A N and Yerin Y S 2011 *J. Low Temp. Phys.* **37** 667–77

[37] Izyumov Y A and Laptev V M 1990 *Phase Transit.* **20** 95–112
[38] Piña J C, de Souza Silva C C and Milošević M V 2012 *Phys. Rev.* B **86** 024512
[39] Lin S Z and Bulaevskii L N 2013 *Phys. Rev. Lett.* **110** 087003
[40] Lin S Z and Reichhardt C 2013 *Phys. Rev.* B **87** 100508
[41] da Silva R M, Milošević M V, Domínguez D, Peeters F M and Aguiar J A 2014 *Appl. Phys. Lett.* **105** 232601
[42] Lin S Z 2014 *J. Phys.: Condens. Matter.* **26** 493203
[43] Fenchenko V N and Yerin Y S 2012 *Physica* C **480** 129–36
[44] Vagov A, Shanenko A A, Milošević M V, Axt V M, Vinokur V M, Aguiar J A and Peeters F M 2016 *Phys. Rev.* B **93** 174503
[45] Wolf S, Vagov A, Shanenko A A, Axt V M, Perali A and Aguiar J A 2017 *Phys. Rev.* B **95** 094521
[46] Lin S Z 2012 *Phys. Rev.* B **86** 014510
[47] Yerin Y S and Omelyanchouk A N 2017 *Low Temp. Phys.* **43** 1013–37
[48] Mosquera Polo A S, da Silva R M, Vagov A, Shanenko A A, Deluque Toro C E and Aguiar J A 2017 *Phys. Rev.* B **96** 054517
[49] da Silva R M, Milošević M V, Shanenko A A, Peeters F M and Aguiar J A 2015 *Sci. Rep.* **5** 12695
[50] Salasnich L, Shanenko A A, Vagov A, Aguiar J A and Perali A 2019 *Phys. Rev.* B **100** 064510
[51] Vargas-Paredes A A, Shanenko A A, Vagov A, Milošević M V and Perali A 2020 *Phys. Rev.* B **101** 094516
[52] Vagov A, Shanenko A A, Milošević M V, Axt V M and Peeters F M 2012 *Phys. Rev.* B **85** 014502
[53] Vagov A, Shanenko A A, Milošević M V, Axt V M and Peeters F M 2012 *Phys. Rev.* B **86** 144514
[54] Stanev V and Tešanović Z 2010 *Phys. Rev.* B **81** 134522
[55] Orlova N V, Shanenko A A, Milošević M V, Peeters F M, Vagov A and Axt V M 2013 *Phys. Rev.* B **87** 134510
[56] Yerin Y, Omelyanchouk A, Drechsler S-L, Efremov D V and van den Brink J 2017 *Phys. Rev.* B **96** 144513
[57] Lifshitz E M and Pitaevskii L P 1980 *Statistical Physics, Part 2* (Landau and Lifshitz Course of Theoretical Physics vol 9) (Oxford: Pergamon)
[58] de Gennes P G 1966 *Superconductivity of Metals and Alloys* (New York: Benjamin)
[59] Ketterson J B and Song S N 1999 *Superconductivity* (Cambridge: Cambridge University Press)
[60] Krägeloh U 1969 *Phys. Lett.* A **28** 657–8
[61] Essmann U 1971 *Physica* **55** 83–93
[62] Aston D R, Dubeck L W and Rothwarf F 1971 *Phys. Rev.* **3** 2231–6
[63] Jacobs A E 1971 *Phys. Rev.* B **4** 3029–34
[64] Auer J and Ullmaier H 1973 *Phys. Rev.* B **7** 136–45
[65] Klein U 1987 *J. Low Temp. Phys.* **69** 1–36
[66] Weber H W, Seidl E, Botlo M, Laa C, Mayerhofer E, Sauerzopf F M, Schalk R M and Wiesingerh H P 1989 *Physica* C **161** 272–86
[67] Brandt E H 1995 *Rep. Prog. Phys.* **58** 1465–594
[68] Luk'yanchuk I 2001 *Phys. Rev.* B **63** 174504
[69] Laver M *et al* 2006 *Phys. Rev. Lett.* **96** 167002
[70] Laver M *et al* 2009 *Phys. Rev.* B **79** 014518
[71] Mühlbauer S, Pfleiderer C, Böni P, Laver M, Forgan E M, Fort D, Keiderling U and Behr G 2009 *Phys. Rev. Lett.* **102** 136408
[72] Brandt E H and Das M P 2011 *J. Supercond. Nov. Magn.* **24** 57–67
[73] Pautrat A and Brûlet A 2014 *J. Phys.: Condens. Matter.* **26** 232201
[74] Reimann T, Mühlbauer S, Schulz M, Betz B, Kaestner A, Pipich V, Böni P and Grünzweig C 2015 *Nat. Commun.* **6** 8813
[75] Wang Y, Lortz R, Paderno Y, Filippov V, Abe S, Tutsch U and Junod A 2005 *Phys. Rev.* B **72** 024548
[76] Ge J Y, Gladilin V N, Sluchanko N E, Lyashchenko A, Filipov V, Indekeu J O and Moshchalkov V V 2017 *New J. Phys.* **19** 093020
[77] Neumann L and Tewordt L 1966 *Z. Phys.* **189** 55–66
[78] Neumann L and Tewordt L 1966 *Z. Phys.* **191** 73–80
[79] Fetter A L and Walecka J D 2003 *Quantum Theory of Many-Particle Systems* (New York: Dover)
[80] Jacobs A E 1972 *Phys. Lett.* A **38** 153
[81] Buzdin A I and Kachkachi H 1997 *Phys. Lett.* A **225** 341–8
[82] Houzet M and Buzdin A 2001 *Phys. Rev.* B **63** 184521
[83] Houzet M and Mineev V P 2007 *Phys. Rev.* B **76** 224508
[84] Sigrist M and Ueda K 1991 *Rev. Mod. Phys.* **63** 239–311
[85] Tanaka Y 2015 *Supercond. Sci. Technol.* **28** 034002
[86] Geilikman B T, Zaitsev R O and Kresin V Z 1967 *Sov. Phys. Solid State* **9** 642–7
[87] Kogan V G and Schmalian J 2011 *Phys. Rev.* B **83** 054515
[88] Bogomolnyi E B 1976 *Sov. J. Nucl. Phys.* **24** 449–54
[89] Brinkman A, Golubov A A, Rogalla H, Dolgov O V, Kortus J, Kong Y, Jepsen O and Andersen O K 2002 *Phys. Rev.* B **65** 180517(R)
[90] Lubashevsky Y, Lahoud E, Chashka K, Podolsky D and Kanigel A 2012 *Nat. Phys.* **8** 309–12
[91] Poole C P, Farach H A, Creswick R J and Prozorov R 2014 *Superconductivity* (Amsterdam: Elsevier)
[92] Wolf S, Vagov A, Shanenko A A, Axt V M and Aguiar J A 2017 *Phys. Rev.* B **96** 144515